Journal of Physics: Conference Series **525** (2014) 012024 doi:10.1088/1742-6596/525/1/012024

Effect of surface wettability on carbon nanotube water–based nanofluid droplet impingement heat transfer

Robert Gordon Jackson[a], Mostafa Kahani[a], Nitin Karwa[a], Alex Wu[b], Robert Lamb[b], Robert Taylor[c], Gary Rosengarten[1,a]

[a] School of Aerospace, Mechanical and Manufacturing Engineering, RMIT University, Melbourne, Australia

[b] Department of Chemistry, The University of Melbourne, Parkville, Australia

[c] School of Mechanical and Manufacturing Engineering, The University of New South Wales, Kensington, Australia

E-mail: gary.rosengarten@rmit.edu.au

Abstract. Recent studies into droplet impingement heat transfer have demonstrated that it has great potential for providing high heat flux cooling in areas such as thermal management of electronics. The wettability of the surface affects the flow dynamics of the impingement process and the resulting heat transfer. In this study, the effect of surface wettability on carbon nanotube water-based nanofluid droplet impingement heat transfer has been studied and compared with water. Superhydrophobic or hydrophilic coatings are applied on one face of monocrystalline silicon wafers (the drop impinges on this face) while the other face is painted matt black to permit infrared thermography. The silicon wafer is preheated to 40 °C and a single droplet impinges normally on the top facing coated surface of the monocrystalline silicon wafer. The inverse heat conduction problem has been solved using the measured black face temperature. For both the water and nanofluid droplets, the convective heat transfer coefficient reduces with the decrease in surface wettability. It is found that the nanofluid produce a significantly higher convective heat transfer coefficient during droplet impingement than water, with the enhancement increasing with increasing wettability.

1. Introduction

There are a large number of applications that require high heat-flux cooling, such as thermal management on high-powered chips, fire suppression and the rapid quenching of steel. Droplet impingement, particularly in the form of spray cooling, has been shown to be an effective means of rapid heat removal. Spray cooling involves heat transfer to multiple droplets impinging simultaneously and in rapid succession over a large area. This method of cooling is capable of providing high heat transfer coefficient like impinging jets, but with a mass flux as much as one order of magnitude less [1,2]. Spray cooling can either occur as non-boiling or evaporative/boiling. Higher heat flux can be achieved through boiling and evaporation, but non-boiling heat transfer systems are more suited for electronics cooling applications as the system is less complex. Karwa et al. [2] reported a non-boiling heat transfer coefficient of 25000 W/m^2·K for mass flux of 9.94 kg/m^2·s. Wang et al. [3] reached an

[1] To whom any correspondence should be addressed.

even higher non-boiling heat transfer coefficient of 66000 W/m^2·K for mass flux of 53 kg/m^2·s but reported that a thick fluid film remains on the surface.

A nanofluid is a suspension of particles, less than 100 nm in size, within a liquid. The particles can be used to tailor the fluid properties. For example, for better thermal properties than the base liquid, double-walled carbon nanotube nanoparticles (k~2000 W/m·K [4]) are added to water (k~0.607 W/m·K) in concentration of just 0.6% w/w, and the resulting thermal conductivity of the nanofluid is 34% higher than that of water [5]. The thermal conductivity of the nanofluid is a function of the thermal conductivities, particle sizes and relative concentrations of the constituent media. Patel et al. [6] suggested the following equation for the thermal conductivity of carbon nanotube water-based nanofluid

$$k_{nf} = k_f \left[1 + \frac{k_p \varphi r_f}{k_f (1-\varphi) r_p}\right]. \quad (1)$$

The dynamic viscosity can be found using the correlation [7]

$$\mu_{nf} = \mu_f (1 + 22.7814\varphi - 9748.4\varphi^2 + 1\,000\,000\varphi^3). \quad (2)$$

The density and specific heat capacity are calculated as

$$\rho_{nf} = \varphi \rho_p + (1-\varphi)\rho_f, \quad (3)$$

$$C_{p_{nf}} = \varphi C_{p_p} + (1-\varphi) C_{p_f}. \quad (4)$$

The dynamics of droplet impingement depends on various factors, such as the Weber number of the droplet, the Reynolds number of the flow during impact, and the wettability of the surface (the equilibrium contact angle between the droplet and the impingement surface is a measure of the surface wettability) [8]. Rosengarten et al. [9] have shown that the surface contact angle influences the maximum spreading diameter of the droplet, contact time and effectiveness of heat transfer; for single droplet impingement events, it was observed that hydrophilic surfaces (contact angle < 25°) offer a higher cooling effectiveness than both uncoated (contact angle ~ 90°) and superhydrophobic surfaces (contact angle > 160°). If this is also true for a nanofluid, then it will provide an additional means by which heat transfer can be enhanced. Relevant studies on the effect of surface wettability on the nanofluid droplet impingement are not available.

In the present investigation, the effect of surface wettability on heat transfer to a carbon nanotube water-based nanofluid droplet and the enhancement with respect to water is determined.

2. Experimental apparatus and method

Figure 1a shows the schematic layout of the experimental setup. A photograph of the experimental setup is shown in Figure 1b. Wafers of monocrystalline silicon were used as the impingement targets due to the high rigidity and thermal conductivity of silicon. Each wafer was 0.5 mm thick and 100 mm in diameter. The undersides of the wafers were coated with a matte black spray paint allowing temperature measurement by thermal imaging camera. Coatings were applied to the topside of the silicon wafers to modify the surface wettability; one was given a superhydrophobic coating, one was given a hydrophilic coating and the third wafer was left uncoated as the reference surface. The wafer is heated by warm air rising from a ring heater. The ring heater also allows unobstructed view of the bottom surface for thermal imaging.

The superhydrophobic coating was comprised of a mixture of silica nanoparticles (Evonik), dimethylsiloxane polymer (Gelest) and methyltrimethoxysilane (Sigma-Aldrich) as the linking agent. This is produced and applied to the silicon wafers by the methods described in [10]. The hydrophilic coating was prepared in the same way, except that tetraethoxysilane is used as the linking agent with an ethoxylated siloxane polymer. The surface roughness of the superhydrophobic surface was measured to have an RMS value of 308 nm and a roughness ratio of 1.5 [9].

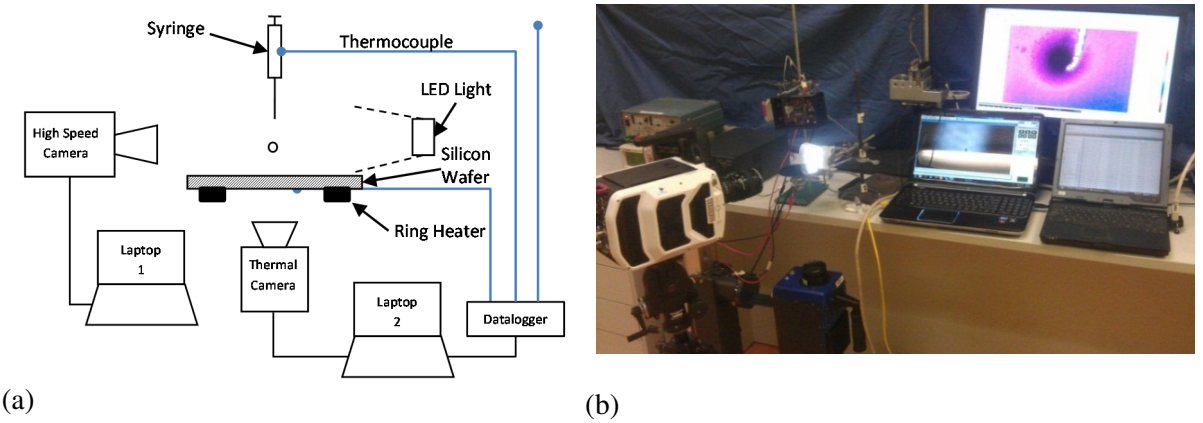

Figure 1. a) Schematic of the experimental setup, **b)** Photograph of the experimental setup.

Double-walled carbon nanotubes (DWCNT) (Sigma Aldrich) with an average diameter of 3.5 nm and a mean length of 1–10 μm were dispersed in Type 1 water to form DWCNT/water nanofluid. Sodium dodecyl sulphate (SDS) was employed as the dispersant. DWCNT and SDS powders were added to Type 1 water while stirring with a magnetic stirrer for an hour, the suspensions were then sonicated for 35 minutes. Nanofluids were prepared with DWCNT particle concentrations of 0.25, 0.5 and 0.75% w/w. Weight fractions are calculated by dividing the mass measured for the CNT nanoparticles by the final nanofluid mass, using an analytical balance with 0.01 mg resolution (Ohaus Discovery Semi-Micro). Mass fraction can be converted to volume fraction using the following equation:

$$v/v\% = \frac{w/w\%}{w/w\% + (1 + w/w\%)\rho_p/\rho_f} \quad (5)$$

The concentration of surfactant in these nanofluids was 0.25, 0.50 and 0.75% w/w, respectively. The samples were left stationary for 7 days and thereafter were found to be sufficiently stable with no visually observable sedimentation. The thermal properties of the three different concentration nanofluids are calculated using Eq. 1–4 and are shown in Table 1. The predicted enhancement in thermal conductivity of these nanofluids is higher than the range shown in Patel et al. [6] because the diameter of the CNTs used is different. Patel et al. [6] uses CNTs with an average diameter of 30nm, while the CNTs used here have an average diameter of 3.5nm (Sigma Aldrich). Low concentrations of carbon nanotube nanoparticles, such as those used in this experiment, do not cause the surface tension of the nanofluid to differ significantly from that of the base fluid [11], so the surface tension is assumed to be the same as that of an equivalent water/SDS solution. Elworthy and Mysels [12] provide data showing the surface tension of water containing various concentrations of SDS; at a mass concentration of 0.25% the surface tension is 39.5 mN/m, this decreases to 38.5 mN/m as the concentration is increased to 0.75%.

Table 2 shows the wettability of water and nanofluid on the various surfaces. Contact angle measurements were taken from images of the droplets taken using the high-speed camera after the droplet had become sessile. The image of the droplet was processed in Matlab by firstly extracting the pixels representing the droplet from the surrounding image, then drawing a line tangent to the first five pixels that described the curvature of the top of the droplet. The maximum error for this process is for contact angles close to 90°, where the error is ±5.5°. For superhydrophobic (γ>165°) and hydrophilic (γ<15°), the error is less than ±0.4°. As can be seen, the only property of water that significantly changes at these nanoparticle concentrations is the thermal conductivity and the contact angle. Most importantly, the nanofluid is able to wet the hydrophobic surface. This means that the thermohydraulics of nanofluid droplet impingement will be different than a water droplet. Also, it is not known how a nanofluid fundamentally interacts with a superhydrophobic surface.

Table 1. Thermal and transport properties for water, carbon nanotube nanoparticles and nanofluid.

		Water	DWCNT	0.25% w/w		0.50% w/w		0.75% w/w	
				Nanofluid	% Difference	Nanofluid	% Difference	Nanofluid	% Difference
k	W/(m·K)	0.607	2000	0.7427	22.36	0.8778	44.6054	1.0121	66.7421
μ	kg/(m·s)	8.9×10^{-4}	-	0.0009	1.4975	0.0009	1.2591	0.0009	0.2911
ρ	kg/m^3	997	2100	998.31	0.1312	999.61	0.2615	1000.90	0.3908
c_p	J/(kg·K)	4180	530	4175.67	-0.1036	4171.37	-0.2064	4167.11	-0.3084
γ	mN/m	72.8	-	39.5	-45.7	38.8	-46.7	38.5	-47.1

Table 2. Wettability of water and nanofluid on test surfaces.

Surface coating	Surface contact angle (degrees)			
	Water	0.25% w/w	0.50% w/w	0.75% w/w
Hydrophilic	25	11.0	8.4	11.5
Uncoated	43	10.9	7.2	11.5
Superhydrophobic	165	81.8	59.5	58.9

A 30 gauge needle (OD 0.31 mm, ID 0.16 mm) was fixed onto a syringe and its tip was 100 mm above the silicon wafer. A thermocouple was installed in-line between the syringe and needle to measure the temperature of the droplet immediately at the moment of dispensation. A second thermocouple was hung near the apparatus to measure the ambient air temperature. A third thermocouple was attached to the bottom of the silicon wafer to measure the wafer temperature during IR camera calibration. A National Instruments NI9219 analogue input data logger recorded the temperature data at a rate of 10 kHz and passed this to a laptop running LabView.

A FLIR Titanium thermal imaging camera was mounted beneath the silicon wafer to view the black-painted underside. This was connected to a laptop running the FLIR Altair recording and analysis software. The camera was configured to run at 870 fps, with a 1 ms integration time and a resolution of 160×128 pixel[2]. The sensor in the camera was calibrated using a thermocouple attached to the wafer over a temperature range of 17–49 °C.

The droplet travel path from the needle to the impingement surface was back illuminated by a high-powered LED light fitted with a diffuser. A Phantom v1610 high-speed camera was used to image the impingement phenomenon from the side. The camera was configured to record at 8700 fps, a multiple of the thermal camera's frame rate.

The wafer was heated until it reached a stable temperature of approximately 40°C. A droplet was dispensed from the syringe onto the heated wafer. The thermal and high-speed cameras simultaneously recorded the droplet impingement process. After each droplet impingement, the surface was rinsed with Type 1 water, allowed to dry and then reheated. This process was repeated three times for each concentration of the nanofluid and for each surface coating.

3. Data Analysis

The high-speed visible images are processed in MATLAB to determine the contact line diameter as it spreads on wafer. Using the Altair thermal camera software, the IR intensity values recorded by the camera were converted to temperature. The temperature data was averaged over a 1 mm diameter circular area around the stagnation point (shown by a blue circle in Fig. 2). From this measured temperature, the impingement face temperature and heat flux are calculated by solving the inverse heat

conduction problem. This calculation is performed using the FORTRAN code presented in § 18.5 of [13], which solves the following equations:

$$T(L,t) = T(0,t) + \sum_{n=1}^{\infty} \frac{1}{(2n)!}\left(\frac{L^2}{\alpha}\right)^n \frac{d^n T(0,t)}{dt^n}, \tag{6}$$

$$q(t) = k\sum_{n=1}^{\infty} \frac{L^{2n-1}}{(2n-1)!}\frac{1}{\alpha^n}\frac{d^n T(0,t)}{dt^n}. \tag{7}$$

The instantaneous convective heat transfer coefficient due to droplet impingement can be calculated as

$$h(t) = \frac{q(t)}{T(L,t) - \bar{T}_{drop}}. \tag{8}$$

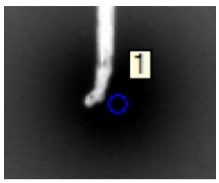

Figure 2. Area-averaged temperature measurement being conducted in Altair. The white object is the thermocouple. The blue circle is 1 mm in diameter and is centered at the thermal footprint on the impinging droplet. The instantaneous wafer temperature for all heat transfer calculations is determined by averaging the temperature over an area enclosed by this circle.

4. Results and discussion

The images in Figure 3 show simultaneous optical and thermal views of the droplet impingement process for water and 0.5% w/w concentration nanofluid droplets on an uncoated silicon surface. The variation of droplet spreading diameter normalized with the initial droplet size is shown in Fig. 4. As the water droplet impacts the wafer surface, its vertical momentum is redirected radially, causing the droplet to flatten and rapidly spread outwards. Surface tension and viscous forces decelerate the radial flow and stop the droplet spreading after approximately 3 ms; this is the maximum diameter to which the droplet spreads, called the equilibrium diameter. Thereafter, the surface contact line remains pinned as the fluid lacks the energy necessary to overcome the adhering forces of the surface but the fluid within the droplet continues to oscillate. First, aided by surface tension pulling the fluid back towards the centre, the internal flow is directed radially inwards. As all of the fluid converges at the centre of impact, an upwash appears at about 9 ms after impact. After reaching the centre the flow reverses, moving the main bulk of the fluid towards the outer edge of the droplet again, although it does not spread beyond the initial maximum diameter. The fluid continues to oscillate between the outer edge and the centre, but the amplitude of the upwash reduces with each oscillation as the flow energy is dissipated by viscous forces. After approximately 30 ms, no fluid motion within the droplet motion is detected.

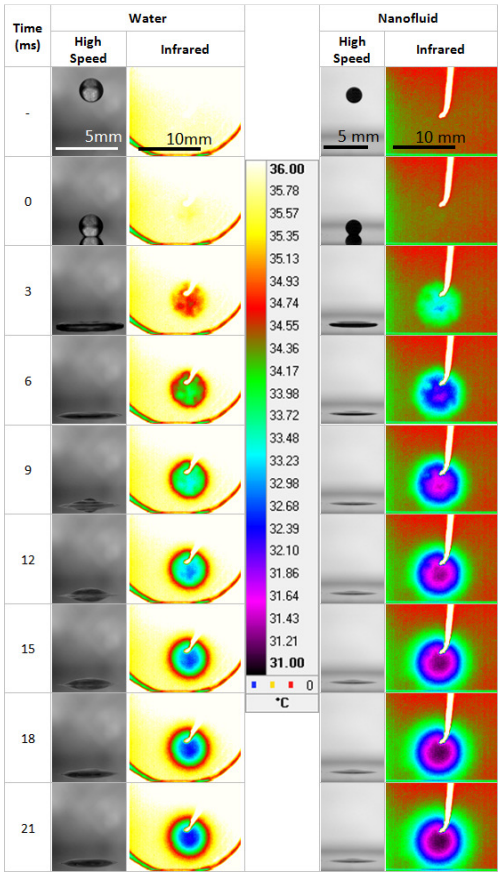

Figure 3. High-speed and infrared images of water (left) and 0.5% w/w concentration nanofluid (right) droplet impingement onto an uncoated silicon surface.

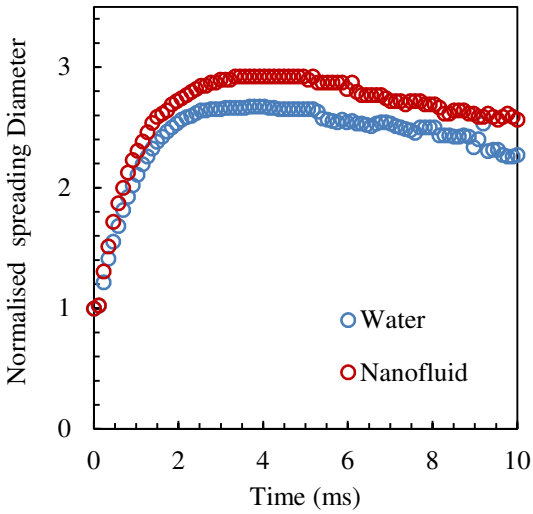

Figure 4. Normalised droplet diameter over time for water and 0.5% w/w concentration nanofluid droplets impinging onto an uncoated surface.

The initial dynamics of the nanofluid droplet impact is similar to those of the water droplet; it spreads rapidly upon coming into contact with the surface, reaching a maximum diameter after 3 ms. However, the nanofluid droplet does not rebound towards the centre as strongly as the water (compare the droplet in Figure 3 at 9 ms). Fluid motion in the nanofluid droplet ceases by 12 ms as compared to 30 ms for the water droplet, which may be due to the lower surface tension of the nanofluid.

Thermal images are shown to the right of the high speed images; these show the temperature of the underside of the wafer as it changes over the course of the droplet impact. Prior to impact, the wafer temperature is uniform. The impingement of the droplet on top of the silicon surface leads to the decrease in surface temperature of a circular area on the bottom face of the wafer; this area is approximately of the same size and shape as the contact area between the droplet and the surface. The cooled area increases in diameter over time, but its growth rate decreases as the droplet spreading velocity decreases. The centre of the circular area is the stagnation point and has the lowest temperature. The wafer temperature increases in the radially outwards direction due to decrease in the convective heat transfer rate.

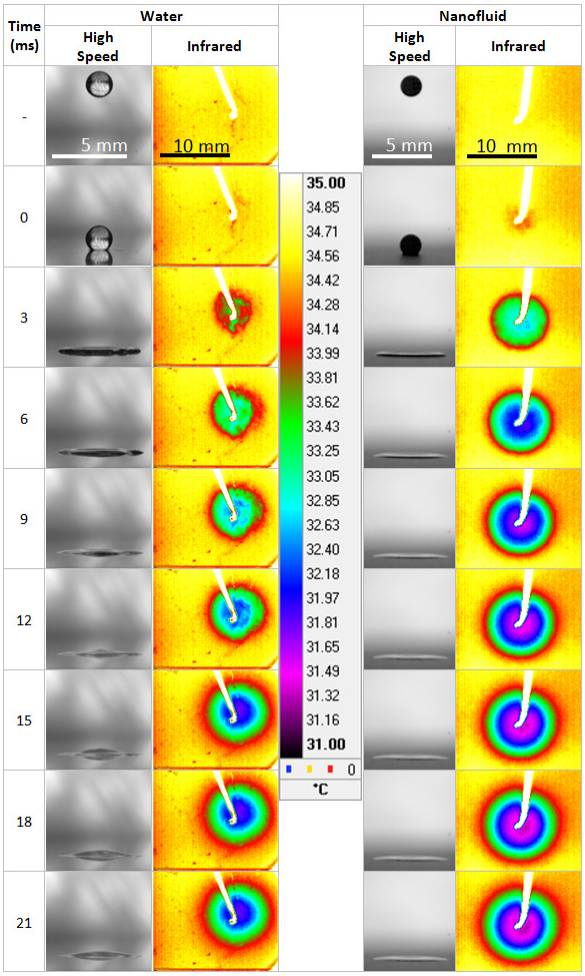

Figure 5. High-speed and infrared images of water (left) and 0.5% w/w concentration nanofluid (right) droplet impingement onto a hydrophilic surface.

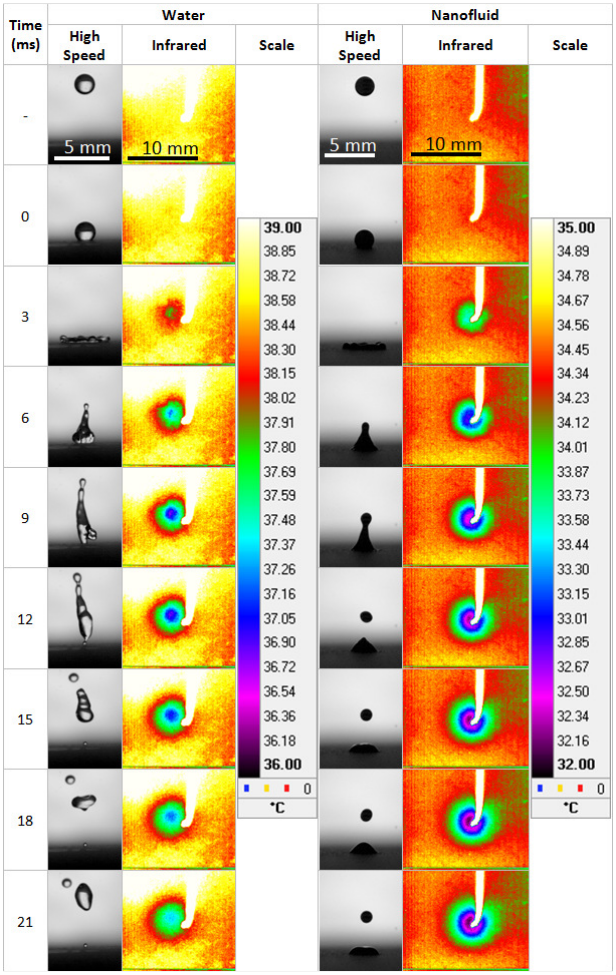

Figure 6. High-speed and infrared images of water (left) and 0.5% w/w concentration nanofluid (right) droplet impingement onto a superhydrophobic surface.

Figure 5 shows water and nanofluid droplet impinging onto hydrophilic surfaces. The area affected by the nanofluid droplet is larger than the size of the area affected by the water droplet. The temperature difference caused by the nanofluid droplet is greater than the temperature difference caused by the water droplet at each point in time. Both of these factors, the size of the area affected and amount of temperature change, indicate that the nanofluid droplet removed more heat from the surface than the water droplet.

Figure 6 shows droplets impinging onto a superhydrophobic surface. After the water droplet has impacted and spread, it rapidly retracts back towards the centre and forms a vertical jet with sufficient momentum to lift the entire droplet off the surface and rebounds. In air, surface tension forces attempt to change its shape into a sphere again. Resultantly, the droplet only stays in contact with the surface for about 9 ms. The thermal image for the water droplet shows that no further cooling is performed after this time and the plate begins to return to its initial temperature as heat from the surrounding solid is conducted towards the cooled spot. The nanofluid droplet impinging onto the superhydrophobic surface does not have as much surface tension as the water droplet, and as such does not rebound as strongly. This results in a significant amount of the nanofluid remaining in contact with the surface, with only a small volume separating as a secondary droplet (visible at 12 ms in Figure 6).

To compare the cooling performance of the two fluids on the three different wafers, the surface temperature is written in a non-dimensional form as

$$\theta = \frac{T_s(0) - T_s(t)}{T_s(0) - T_{drop}(0)} \tag{9}$$

where the surface temperature $T_s(t)$ was the instantaneous average temperature (see in Fig. 2). The variation of θ_0 with time for water and nanofluid for the three surfaces is shown in Fig. 7. For all three surface types, the nanofluid droplet reduces the non-dimensional surface temperature more rapidly than the water droplet does. It can be concluded that nanofluid is more effective at droplet impingement cooling than water. The contact angle between the surface and droplet appears to have a significant effect on the rate at which heat is transferred. Using the uncoated surface as a reference for comparing heat transfer rates, the superhydrophobic surface transfers less heat over time while the hydrophilic surface transfers more heat over time. The low level of heat transfer that results from droplets impinging onto the superhydrophobic surface is due to the small contact area and short contact time. The high-speed images in Figure 6 show the rebounding water droplet loses contact with the surface sometime between 9 and 12 ms, and resultantly the convective heat transfer drops significantly. This can also be seen in the graphs of dimensionless diameter against time shown in Figure 8; by 8 ms the water droplet has returned to a dimensionless diameter of 1, indicating that the droplet is about to lose contact with the surface. The graphs also indicate that the superhydrophobic surface causes a smaller maximum spreading diameter than the other surface types.

The variation of convective heat transfer coefficient over time is shown in Fig. 9. The nanofluid droplets consistently produce a higher convective heat transfer coefficient than water. This is due to the higher thermal conductivity of the nanofluid and the lower surface tension. The peak heat transfer coefficient for nanofluid is particularly high for the hydrophilic surface, approximately three times greater than it is for water. The poor thermal contact between the droplet and superhydrophobic surface results in a peak convective heat transfer coefficient that is significantly lower than for any other surface type. The heat transfer to the water droplet stops about 8 ms after impact because at this point the droplet has left the surface and is therefore no longer cooling it. The nanofluid droplet remains on the surface and continues to cool the surface. Overall, the enhancement in heat transfer rate by nanofluid is least for the hydrophobic surface. The effect of different nanofluid concentration on heat transfer enhancement on an uncoated surface is shown in Figure 10. Note that the surfactant concentration increases in the same proportion as the nanoparticles. While it was expected that increase in the concentration of both would lead to increase in the heat transfer coefficient, the results show that there is no net change in the enhancement factor with the change in nanofluid concentration. The reason for this is not understood at this time and further research in this area is required, with specific emphasis on separating the effect of surfactant and nanoparticle concentration.

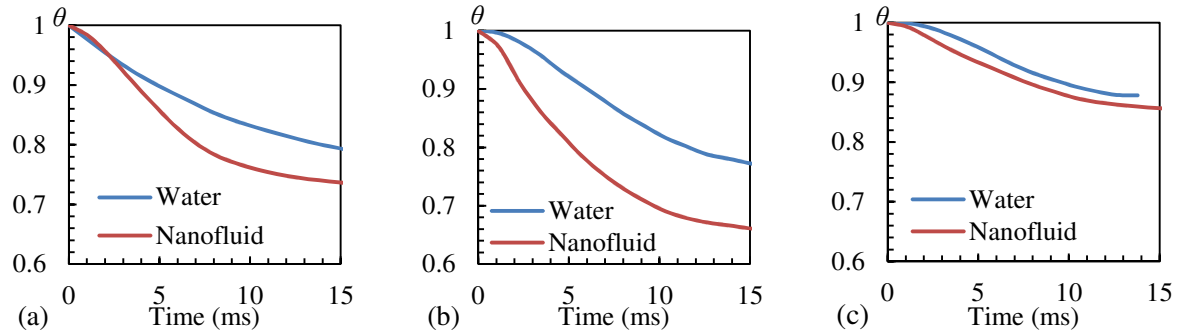

Figure 7. Normalised surface temperature over time for water and 0.5% w/w concentration nanofluid droplets impinging onto (a) uncoated, (b) hydrophilic and (c) superhydrophobic surface.

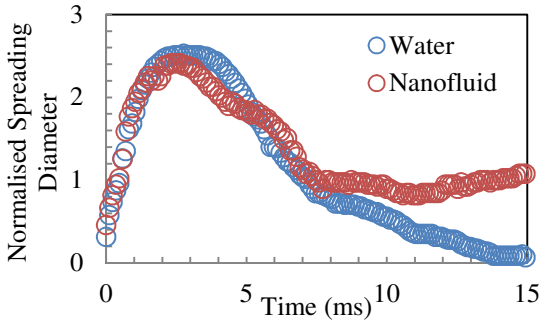

Figure 8. Normalised droplet diameter over time for water and 0.5% w/w concentration nanofluid droplets impinging onto a superhydrophobic surface.

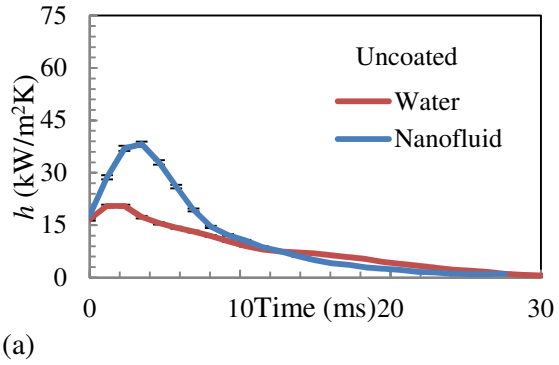

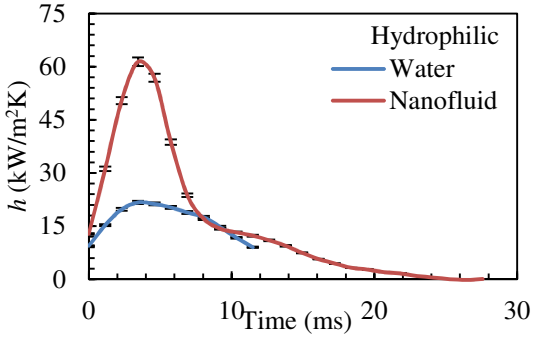

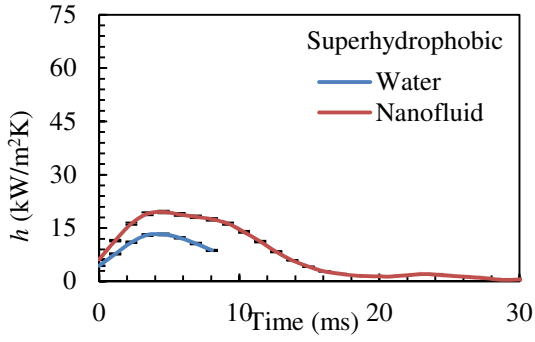

Figure 9. Convective heat transfer coefficient of water and 0.5% w/w concentration nanofluid droplets impinging onto (a) uncoated, (b) hydrophilic and (c) superhydrophobic surface.

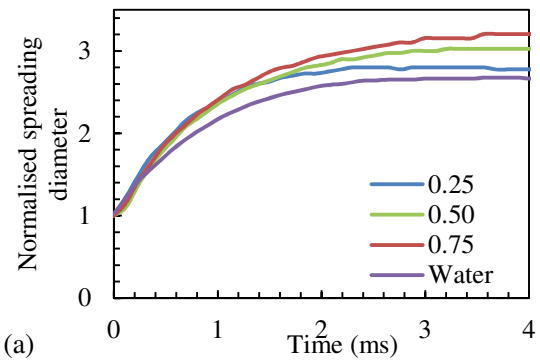

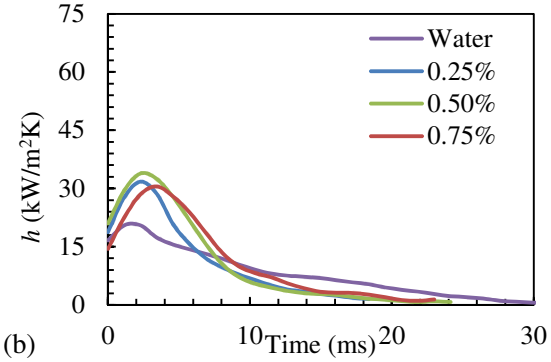

Figure 10. Effect of nanoparticle concentration on droplet spreading and convective heat transfer coefficient on a uncoated surface.

5. Conclusions

Experiments were performed to study the effect of surface wettability on droplet impingement heat transfer to both water and nanofluid. The key findings from the study are

1. The convective heat transfer coefficient of nanofluid droplets is significantly higher than that of water droplets due to its higher thermal conductivity and lower surface tension.
2. Poor wettability of surface results in reduction of heat transfer rate.

These preliminary studies show that the wettability has a major effect on the heat transfer phenomenon. However, no change in the heat transfer rate was observed with the change in nanoparticle concentration. The reason for this observation is not clear and requires further investigation with specific emphasis on separating the effect of surfactant and nanoparticle concentration. The present heat transfer analysis is only one dimensional and does not account for the radial heat conduction within the wafer. A two-dimensional analysis will be performed in the future to determine the distribution of heat transfer coefficient on the surface. Furthermore, the spreading area on the three surfaces is different and it is worthwhile to determine the total heat removed by a droplet.

6. Nomenclature

		Greek Letters		Subscripts	
c_P	Specific heat capacity	α	Thermal diffusivity	*drop*	Droplet
k	Thermal conductivity	γ	Surface tension	*f*	Continuous fluid
L	Wafer thickness	μ	Dynamic viscosity	*nf*	Nanofluid
q	Heat flux	ρ	Density	*p*	Nanoparticle
r	Particle radius	τ	Dimensionless time	*s*	Top surface of silicon wafer (the impingement face)
T	Temperature	φ	Volume fractions		
		θ	Dimensionless temperature		

7. References

[1] Oliphant K, Webb B and McQuay M 1998 *Exp. Therm Fluid Sci.* **18(1)** 1–10.
[2] Karwa N, Kale S R and Subbarao P M V 2007 *Exp. Therm Fluid Sci.* **32** 571–579.
[3] Wang Y, Liu M, Liu M and Xu K 2011 *Heat Transfer Eng.* **32**(11–12) 1075–1081.
[4] Kahani M, Zeinali Heris S and Mousavi S M 2013, *Ind. Eng. Chem. Res.* **52(36)** 13183–13191.
[5] Assael, M J, Metaxa I N, Arvanitidis J, Christofilos D and Lioutas C 2005 *Int. J. Thermophys.* **26(3)** 647–664.
[6] Patel H E, Anoop K B, Sundararajan T and Das S K 2008 *Bull. Mater. Sci.* **31(3)** 387–390.
[7] Ebrahimnia-Bajestan E and Niazmand H 2011 *Iran J Chem. Eng.* **8**(2) 81–97.
[8] Vadillo D C, Soucemarianadin A, Delattre C and Roux D C D 2009 *Phys. Fluids* **21(12)** 122002.
[9] Rosengarten G, Tetuko A, Li K K, Wu A and Lamb R 2011 *ASME Int. Mechanical Eng. Congress*, *Denver*.
[10] Jones A, Lamb R N and Zhang H 2004 US 6,743,467 B1.
[11] Tanvir S and Qiao L 2012 *Nanoscale research letters*, **7**(1) 1-10
[12] Elworthy PH and Mysels KJ 1966 *Journal of colloid and interface science*, **21**(3) 331-347
[13] Taler J and Duda P 2010 *Solving Direct and Inverse Heat Conduction Problems* (Springer).